

# EVRNet: Efficient Video Restoration on Edge Devices

Sachin Mehta<sup>\*1</sup>, Amit Kumar<sup>2</sup>, Fitsum Reda<sup>2</sup>, Varun Nasery<sup>2</sup>, Vikram Mulukutla<sup>2</sup>, Rakesh Ranjan<sup>2</sup>, and Vikas Chandra<sup>2</sup>

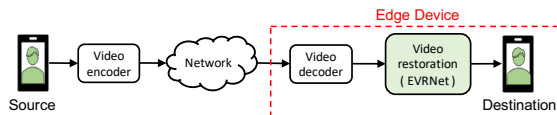
<sup>1</sup>University of Washington    <sup>2</sup> Facebook Inc.

## Abstract

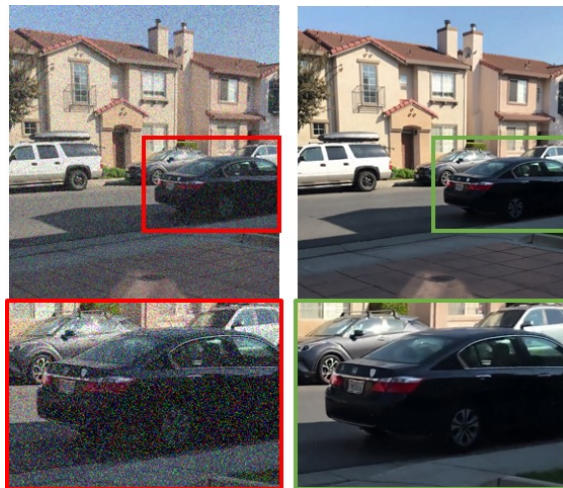
Video transmission applications (e.g., conferencing) are gaining momentum, especially in times of global health pandemic. Video signals are transmitted over lossy channels, resulting in low-quality received signals. To restore videos on recipient edge devices in real-time, we introduce an efficient video restoration network, EVRNet. EVRNet efficiently allocates parameters inside the network using alignment, differential, and fusion modules. With extensive experiments on video restoration tasks (deblocking, denoising, and super-resolution), we demonstrate that EVRNet delivers competitive performance to existing methods with significantly fewer parameters and MACs. For example, EVRNet has  $260\times$  fewer parameters and  $958\times$  fewer MACs than enhanced deformable convolution-based video restoration network (EDVR) for  $4\times$  video super-resolution while its SSIM score is 0.018 less than EDVR. We also evaluated the performance of EVRNet under multiple distortions on unseen dataset to demonstrate its ability in modeling variable-length sequences under both camera and object motion.

## 1. Introduction

Video restoration aims at recovering the expected quality of videos in recipient devices. Deep neural network-based solutions [11, 25, 51, 55, 59] achieve high accuracy on these tasks, but they are computationally very expensive. For example, a deformable convolution-based video restoration network, EDVR [51], has 21.1 million parameters and requires 9.96 TMACs (multiplication-addition operations) for up-sampling a 360p video frame by a factor of 4. Many video transmission applications (e.g., video streaming and video conferencing) run on edge devices, such as smartphones. The trend is likely to continue with the on-going global health pandemic and the need for remote and virtual



(a) EVRNet in video conferencing application.



(b) Sample EVRNet results on unseen videos. **Left:** compressed and noisy frames. **Right:** Restored frames.

Figure 1: **EVRNet on edge devices.** (a) shows how EVRNet is integrated to an edge device while (b) shows the results of EVRNet on H264 compressed and noisy (Gaussian + salt and pepper) “unseen” videos. EVRNet is able to restore the videos with multiple artifacts. See Appendix A for more results.

<sup>\*</sup>This work was done as a part of internship at Facebook.

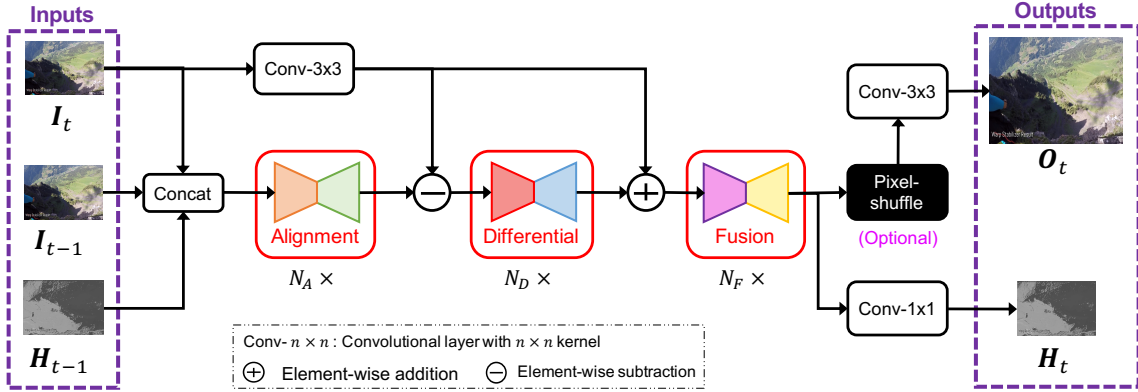


Figure 2: **Overview of the EVRNet architecture for videos.** The EVRNet architecture takes the current RGB  $I_t$ , previous RGB  $I_{t-1}$ , and previous latent  $H_{t-1}$  frames as inputs and produces two outputs: restored RGB frame  $O_t$  and latent frame  $H_t$ . The pixel-shuffle operation is optional and is used only for super-resolution tasks. The alignment, differential, and fusion modules are light-weight and efficient encoder-decoder networks (see Figure 3) with  $N_A$ ,  $N_D$ , and  $N_F$  layers, respectively.

collaboration. Edge devices have limited computational resources, memory, and energy. As such, heavy networks are not suitable for edge devices. Additionally, video signals at source often undergo lossy compression for transmission under limited network bandwidth (see Figure 1a). Because of compression and transmission noise, the quality of received video signals is low. In order to be effective, these applications should be able to restore high quality and temporally stable videos with low latency on edge devices.

In this work, we propose an efficient and unified neural network (see Figure 2) that restores videos with high quality on edge devices in real-time. Efficient Video Restoration Network, (EVRNet), is inspired by traditional computer vision methods for motion estimation and image enhancement [5, 31, 37]. Briefly, EVRNet uses an alignment module to align current and previous frames without optical flow. High-frequency components (e.g., object edges) are often lost during compression. To restore such details, EVRNet uses a differential and fusion module. The differential module learns representations corresponding to high-frequency components while the fusion module uses these representations along with the input to produce high-quality output (see Figure 1b). EVRNet more efficiently allocates parameters and operations inside each of these modules using small and light-weight encoder-decoder networks.

We evaluate EVRNet’s performance on large scale Vimeo-90K dataset [55] on three restoration tasks: (1) de-blocking, (2) denoising, and (3) super-resolution. EVRNet delivers competitive performance as state-of-the-art methods but with significantly fewer parameters and MACs. For example, on the task of video de-blocking and denoising, EVRNet delivers similar performance to ToFlow [55] but with  $46\times$  and  $13.63\times$  fewer MACs and parameters, respectively. On the task of  $4\times$  video super-resolution, EVR-

Net has slightly lower SSIM score (0.018) than EDVR [51], but has  $260\times$  fewer parameters and  $958\times$  fewer MACs.

To summarize, the main contributions of this paper are:

- A novel efficient video restoration network capable of running at real-time on edge devices.
- A unified neural network, EVRNet, that jointly removes compression and noise artifacts that are prevalent in video transmission pipeline.
- Qualitative and quantitative results along with comparisons with state-of-the-art methods on three video restoration tasks, demonstrating EVRNet’s competitive performance, while having significantly fewer network parameters and MACs.

## 2. Related Work

Designing deep neural networks for image and video restoration tasks is an active area of research. In this section, we first briefly review these approaches followed by efforts in improving the efficiency of neural networks.

**Image and video restoration:** Video de-blocking (e.g., [6, 30, 33, 55, 59]), video denoising (e.g., [25, 33, 55, 58, 59]), and super-resolution (e.g., [3, 7, 19, 23, 26, 29, 41, 48, 50–52]) are three main video restoration tasks that have been studied widely in the literature. Video de-blocking aims at removing artifacts that arises due to image or video compression (e.g., checkerboard patterns). Video denoising aims at removing noise-related artifacts that may arise due to noisy transmission channel (e.g., Internet). Super-resolution aims at producing a high-resolution images/videos from low-resolution images/videos. Most methods are studied on one of these tasks and are computationally very expensive.

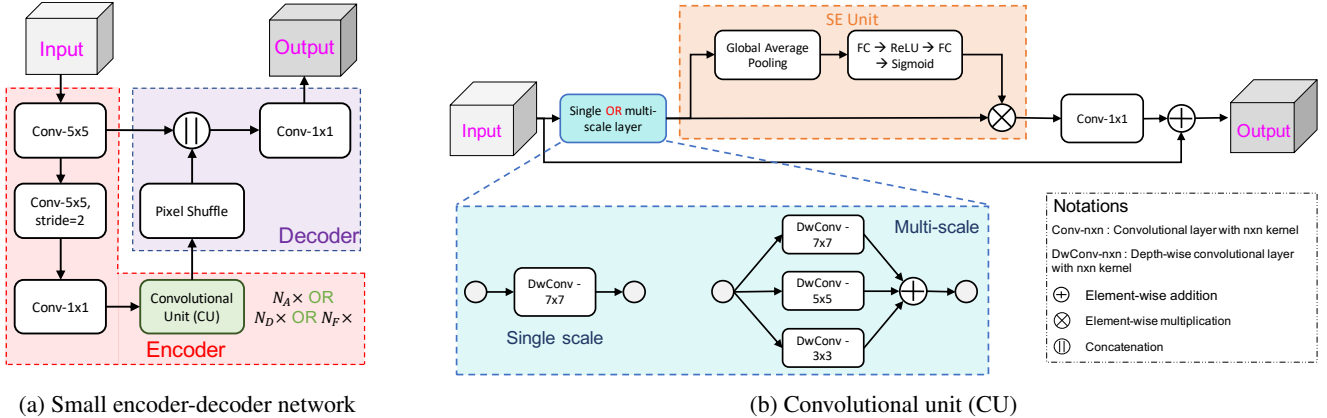


Figure 3: **Overview of alignment, differential, and fusion module.** Each of these modules are identical in construction, i.e., they follow an encoder-decoder structure (a), with an exception to the number of convolutional units (b). The alignment, differential, and fusion module stacks  $N_A$ ,  $N_D$ , and  $N_F$  convolutional units (CUs) to learn deep representations, respectively.

For example, ToFlow [55] has about 466 GMACs for denoising (or deblocking) a 360p video. Also, some video restoration methods use optical flow (e.g., [2, 3, 55]) which is computed using deep flow networks, such as FlowNet [8, 21], PWCNet [43], and SpyNet [38]. Computing optical flow with these networks is expensive and this limits the practical applicability of such approaches, especially on resource-constrained devices (e.g., Smartphones). Similar to [22, 49, 51], EVRNet also does implicit alignment between consecutive frames using the pyramidal structure in the alignment module and handles large motion without optical flow. Importantly, EVRNet can restore videos with high-quality in real-time on edge devices.

**Efficient networks:** Efficient deep neural networks, an active area in both academic and industrial research, aims at reducing the network parameters and MACs by designing efficient learnable layers (e.g., depth-wise convolutions [4]) or quantization or compression or pruning. The most similar to our work are the methods on architecture design (hand-crafted [17, 32, 35, 42] and learned [16, 46, 47, 60]). Similar to these methods, EVRNet also uses depth-wise convolutions for learning representations efficiently. Network compression & pruning (e.g., [10, 14, 27, 36, 53, 57]), quantization (e.g., [1, 20, 39, 54]), and distillation (e.g., [9, 15, 56]) are important complementary efforts that can be further used to improve the efficiency of EVRNet.

### 3. EVRNet

We propose EVRNet, an **Efficient Video Restoration Network**, to remove artifacts and restore videos in edge devices in real-time (schematic shown in Figure 2). EVRNet takes inspirations from traditional techniques in motion estimation and image enhancement [31, 37]. Specifically, EVRNet uses an alignment module based on a pyra-

midal structure to model the motion without explicit use of optical flow. To restore high-frequency details (e.g., edges) that may be lost due to distortions (e.g., compression), EVRNet uses differential and fusion module. These modules learn high-frequency components which are then added back to achieve sharp details. Following sub-sections describe the overall architecture of EVRNet in detail.

#### 3.1. EVRNet Architecture

EVRNet is an auto-regressive network that efficiently models the relationships between a current frame  $\mathbf{I}_t \in \mathbb{R}^{3 \times H \times W}$ , a previous frame  $\mathbf{I}_{t-1} \in \mathbb{R}^{3 \times H \times W}$ , and a previous latent frame  $\mathbf{H}_{t-1} \in \mathbb{R}^{2 \times H \times W}$ . Mathematically, EVRNet takes the form:

$$\mathbf{O}_t, \mathbf{H}_t = \mathcal{F}(\mathbf{I}_t, \mathbf{I}_{t-1}, \mathbf{H}_{t-1}), \quad (1)$$

where  $\mathcal{F}$  is our learned network, EVRNet, that efficiently synthesizes restored frame  $\mathbf{O}_t$  and a latent frame  $\mathbf{H}_t$ , conditioned on inputs ( $\mathbf{I}_t$ ,  $\mathbf{I}_{t-1}$  and  $\mathbf{H}_{t-1}$ ). Overall, EVRNet has three main modules: (1) alignment module, (2) differential module, and (3) fusion module.

**Alignment module:** The alignment module takes a concatenation of the inputs ( $\mathbf{I}_t$ ,  $\mathbf{I}_{t-1}$  and  $\mathbf{H}_{t-1}$ ) and produces aligned representations  $\mathbf{A}_t \in \mathbb{R}^{d \times H \times W}$  using an efficient and light-weight encoder-decoder network (Figure 3a). The alignment module first learns pyramidal representations using the encoder network. These representations are then combined by the decoder to produce aligned representations. Compared to existing methods that learns very deep pyramidal representations for motion estimation [8, 21, 31, 38, 43], EVRNet is very light-weight and shallow. To demonstrate the ability of EVRNet in modeling the motion, an example is shown in Figure 4 where person moves his head during a conversation. The most salient regions be-

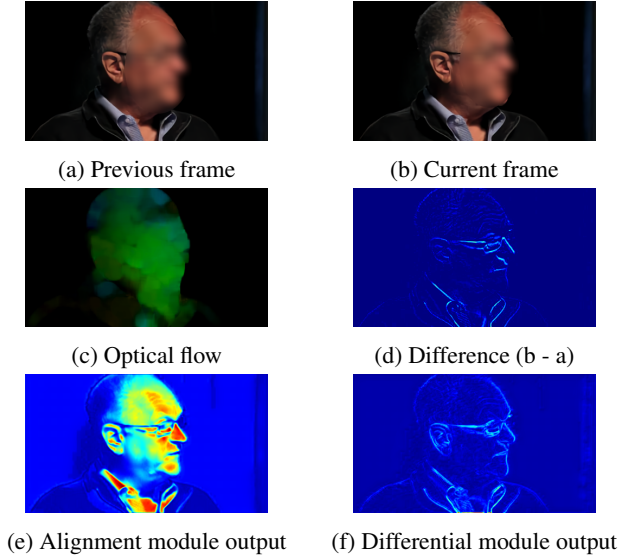


Figure 4: This example visualizes outputs of two EVR-Net modules (alignment and differential). The alignment module pays attention to areas corresponding to motion, i.e., nose and spectacles (c, d vs. e) while the differential module pays attention to high frequency components (e.g., spectacle edges in (f)) in region corresponding to motion.

tween consecutive frames are near the nose, spectacles, and shirt as depicted by the optical flow and difference image in Figure 4c and 4d, respectively. The alignment module in the EVRNet also pays attention to these salient regions (red color regions in Figure 4f), illustrating that EVRNet can model the motion implicitly.

Specifically, the encoder in the alignment module consists of (a) a  $5 \times 5$  standard convolutional layer, (b) a  $5 \times 5$  standard convolutional layer with a stride of 2, (c) a point-wise convolutional layer, and (d)  $N_A$  convolutional units (CUs; Section 3.2), where  $N_A$  controls the depth of alignment module. The decoder follows a simplified UNet-like architecture [40]. The output of the last convolutional unit (CU) is first upsampled and then concatenated with the output of the first  $5 \times 5$  convolutional layer. The resultant output is then fused using a point-wise convolution to produce aligned representations  $\mathbf{A}_t$ .

**Differential module:** The differential module aims at learning high-frequency components in an image such as object edges. To do so, the input  $\mathbf{I}_t$  is first projected to the same dimensionality as  $\mathbf{A}_t$  using a  $3 \times 3$  convolutional layer to produce a projected output  $\mathbf{P}_t \in \mathbb{R}^{d \times H \times W}$ . An element-wise difference is then computed between  $\mathbf{P}_t$  and  $\mathbf{A}_t$ . The resultant output is then fed to differential module to further refine these representations and produce high-frequency representations  $\mathbf{D}_t \in \mathbb{R}^{d \times H \times W}$ . Figure 4f shows an example where EVRNet pays attention to high-

frequency components (e.g., spectacle and ear edges). Similar to the alignment module, the differential module also takes the form of small and light-weight encoder-decoder network, with an exception to number of CUs. In the differential module, we stack  $N_D$  CUs.

**Fusion module:** The fusion module combines high-frequency representations obtained from the differential module  $\mathbf{D}_t$  with projected input representations  $\mathbf{P}_t$  and produces restored frame  $\mathbf{O}_t$  and latent frame  $\mathbf{H}_t$ . We first add  $\mathbf{D}_t$  with  $\mathbf{P}_t$  to enhance high-frequency components and then feed the resultant tensor to a fusion module. If the spatial dimensions of  $\mathbf{O}_t$  are not the same as  $\mathbf{I}_t$  (e.g., in super-resolution), the output of fusion module is up-sampled using a pixel-shuffle operation. Otherwise, an identity operation is performed. The resultant output is then convolved with a  $3 \times 3$  convolutional layer to produce  $\mathbf{O}_t$ . In parallel, the output of fusion layer is also projected using a point-wise convolutional layer to produce latent frame  $\mathbf{H}_t$ . Similar to the alignment and differential module, the fusion module is also an efficient and light-weight encoder-decoder network with  $N_F$  CUs.

The operation of differential and fusion module is similar to traditional image enhancement methods (e.g., unsharp mask) [5, 37]. In such approaches, the input image is first smoothed to suppress high-frequency components. Then, a difference between smoothed image and input image is computed to identify high-frequency components, which are then added back to the input image to enhance it.

### 3.2. Convolutional Unit (CU)

CNN-based methods for different visual recognition tasks learns representations using either a single branch (e.g., ResNet [13] and MobileNets [17, 42]) or multiple branches (e.g., InceptionNets [44, 45] and ESPNets [34, 35]). We also study these two methods for learning representations. For learning representations at a single scale, we use a depth-wise convolutional layer with  $7 \times 7$  kernel while for learning representations at multiple scales, we apply three depth-wise convolutional layers simultaneously ( $3 \times 3$ ,  $5 \times 5$ , and  $7 \times 7$ ). In both of these methods, the effective receptive field is the same, i.e.,  $7 \times 7$ . Following recent efficient architectures (e.g., MobileNetV3 [16]), we also adopt squeeze-excitation unit (SE unit) [18] to model channel inter-dependencies. Figure 3b sketches the CU.

## 4. Experimental Results

To demonstrate the effectiveness of EVRNet on video restoration tasks, we evaluate its performance on three tasks: (1) deblocking (Section 4.2), (2) denoising (Section 4.3), and (3) super-resolution (Section 4.4). In this section, we first describe the experimental set-up and then evaluate the performance of EVRNet on each of these tasks.



Figure 5: **Performance of EVRNet under compression artifacts.** In (a, b), performance in terms of PSNR and SSIM is measured as a function of compression factor  $Q$  on both RGB and Y frames, respectively. Lower value of  $Q$  means higher compression. In (c), qualitative results for two sample images are shown at different value of  $Q$ . The top and bottom panels corresponds to the compressed frame and restored frames, respectively. Here, PSNR values are computed on RGB frames. See Appendix A.1 for more results.

#### 4.1. Experimental Set-up

**Tasks:** We study three video restoration tasks: (1) *Video deblocking* aims at removing artifacts that may arise due to video compression, (2) *Video denoising* aims at removing noise (e.g., adaptive white gaussian noise (AWGN)) which may be induced during video transmission, and (3) *Video super-resolution* which aims at up-sampling low-resolution video to high-resolution at receiver’s end.

**Dataset:** To evaluate the performance of EVRNet, we use large-scale Vimeo-90K dataset [55] which consists of about 90K independent and diverse video shots with both indoor and outdoor lighting scenarios. We use official training and test splits. Note that, we split the training set randomly into two subsets using 90:10 ratio. The first subset is used for training while the second subset is used for validation.

**Training:** EVRNet models are trained by minimizing L1 loss using ADAM optimizer [24] for 50 epochs (or about 50K iterations) using PyTorch. Based on our ablation experiments in Section 6, we set  $N_A = 5$ ,  $N_D = 2$ , and  $N_F = 2$ . The learning rate is increased linearly from  $1e^{-7}$  to  $1e^{-3}$  in first 100 iterations and is then annealed by half at 15-, 25-, 35-, and 45-th epochs. We train EVRNet with an effective batch size of 64 (8 images per GPU x 8 GPUs) and use a L2 weight decay of  $1e^{-6}$ . All our convolutional layers are followed by a PReLU activation [12], except the activation in multi-scale block is after the addition operation. Standard augmentation methods, such as random crop, random flipping, random gamma correction, and random rotation,

are used during training. Task-specific augmentation methods are included in respective sub-sections. For comparison with existing methods, we use official splits for deblocking, denoising, and super-resolution while for sensitivity studies, we use functions from OpenCV and Skimage libraries.

**Evaluation metrics:** We use two standard quantitative metrics: (1) peak signal-to-noise ratio (PSNR) and (2) structural similarity index (SSIM). Higher value of PSNR and SSIM indicates better performance. Following previous methods, we report these metrics on RGB and Y channel (YCbCr color space).

#### 4.2. Video Deblocking

**Sensitivity study:** We train and evaluate EVRNet for the task of deblocking artifacts. Similar to state-of-the-art methods (e.g., [30, 55]), we compress frames using JPEG2000 compression. During training, we randomly select the compression or quality factor ( $Q$ ) between 10 and 40. During evaluation, we vary the value of  $Q$  from 15 to 90 using OpenCV. Smaller value of  $Q$  indicates higher compression or more blocking artifacts. Note that the same EVRNet network is evaluated at different values of  $Q$ .

Figure 5 shows quantitative and qualitative results under different values of  $Q$ . The quantitative results in Figure 5a and Figure 5b for both RGB and Y-channel shows that EVRNet is robust to compression. For example, at  $Q = 15$ , EVRNet is able to achieve PSNR and SSIM values (RGB space) of 33 dB and 0.91, respectively, indicating that it can

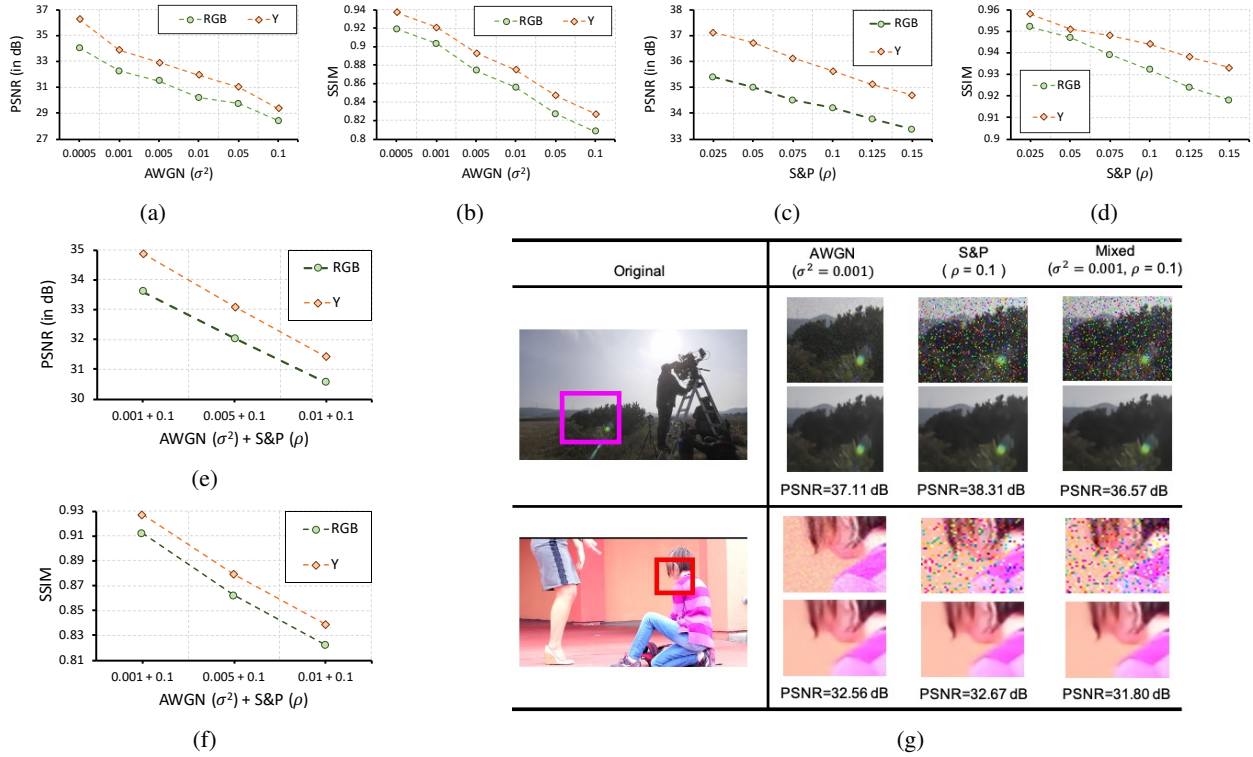


Figure 6: **Performance of EVRNet under noise artifacts.** In (a, b), performance in terms of  $\rho$  PSNR and SSIM is measured as a function of AWGN noise variance  $\sigma^2$  on both RGB and Y frames, respectively. Similarly, in (c, d) and (e, f), performance curves are drawn for salt and pepper noise (S&P) density  $\rho$  and mixed noise (AWGN + S&P). Lower value of  $\sigma^2$  and  $\rho$  means less noise. In (g), qualitative results for two sample images are shown for different types of noise. The top and bottom panels corresponds to the noisy and restored frames, respectively. Here, PSNR values are for RGB frames. See Appendix A.2 for more results.

generate good quality frames even under high compression. These quantitative results are further strengthened with the qualitative results in Figure 5c. The compression artifacts around the hand and strings of harp in the first row and bread loaf in the second row of Figure 5c are completely removed by EVRNet, even under high compression.

**Comparison with state-of-the-art methods:** Table 1 compares the performance of EVRNet with state-of-the-art deblocking methods (ARCNN [6], DnCNN [59], V-BM4D [33], ToFlow [55], and DKFN [30]) on the official Vimeo-90K test set. EVRNet delivers similar or better performance than existing methods while having significantly fewer network parameters and multiplication-addition operations (MACs). For example, EVRNet delivers the similar performance as ToFlow [55], but has  $46\times$  fewer MACs and  $13.64\times$  fewer parameters.

### 4.3. Video Denoising

**Sensitivity study:** Following state-of-the-art methods, we train and evaluate EVRNet under three noise types: (1) Additive White Gaussian Noise (AWGN), (2) Salt and Pepper

Method	MACs	# Params	PSNR	SSIM
ARCNN <sup>†</sup> [6]	27.73 G	117.73 K	36.11	0.960
DnCNN <sup>†</sup> [59]	128.64 G	558.34 K	37.26	0.967
V-BM4D [33]	–	–	35.75	0.959
ToFlow [55]	466.83 G	1073.48 K	36.92	0.966
DKFN [30]	–	–	37.93	0.971
EVRNet (Ours)	10.13 G	78.71 K	36.65	0.967

Table 1: **Comparison with state-of-the-art methods on the task of video deblocking.** EVRNet delivers similar or better performance, but with significantly fewer parameters and multiplication-addition operations (MACs). Here, we report results on the official Vimeo-90K compressed test set where frames are compressed using FFMPEG. See [55] for more details. Similar to previous works, we report results in RGB colorspace. The results of methods marked with <sup>†</sup> are reported in [30] while V-BM4D’s performance is reported in [55]. MACs are measured for  $640 \times 360$  RGB frame.

noise (S&P), and (3) mixture of AWGN and S&P. During training, we randomly select the variance of AWGN noise

$\sigma^2$  between 0.05 and 0.4 and the density of S&P noise  $\rho$  between 0.05 and 0.3. Here,  $\sigma$  represents the standard deviation and the value of  $\rho$  measures the percentage of pixels randomly replaced with noise. For example,  $\rho = 0.3$  indicates that 30% of pixels in a frame are randomly replaced with S&P noise. During evaluation, we first study the effect of AWGN (Figure 6a and 6b) and S&P (Figure 6c and 6d) independently. For AWGN, we vary  $\sigma^2$  between 0.0005 and 0.1 while for S&P, we vary  $\rho$  between 0.025 and 0.15. We then study the effect of mixture of AWGN and S&P noise (Figure 6e and 6f). In these experiments, we set  $\rho = 0.1$  and vary  $\sigma^2$  between 0.001 and 0.1. Note that we train only one EVRNet network for video denoising and then evaluate it at different settings of AWGN, S&P, and mixed noise.

The quantitative results in Figure 6 shows that EVRNet is robust to different types and amounts of noise. For example, the RGB PSNR values of EVRNet with AWGN noise ( $\sigma^2 = 0.001$ ; Figure 6a), S&P noise ( $\rho = 0.1$ ; Figure 6c), and mixed noise ( $\sigma^2 = 0.001$  and  $\rho = 0.1$ ; Figure 6e) are around 33 dB, showing the robustness of EVRNet to different types of noise. This is further demonstrated qualitatively in Figure 6g. In the first and second row of Figure 6g, we can see that EVRNet is able to remove noise and also, restore fine details (e.g., hairs in the second row) under different types of noise.

**Comparison with state-of-the-art methods:** Most state-of-the-art methods train denoising models on Vimeo-90K dataset and evaluate on Vid4 dataset [28]. Following these works, we adopt the same strategy and evaluate on Vid4 dataset. We also compare EVRNet with ToFlow on the official Vimeo-90K denoising dataset. Results are shown in Table 2. EVRNet delivers competitive performance to state-of-the-art methods, but with significantly fewer MACs and parameters. It is worth mentioning that some existing methods (e.g., ToFlow [55] and N2N + F2F [58]) use optical flow, which is either computationally expensive or requires specialized accelerators. Unlike these methods, EVRNet does not require any flow estimation and is suitable for edge devices.

#### 4.4. Video Super-resolution

We train and evaluate EVRNet on video super-resolution ( $2\times$  and  $4\times$ ) task. For training EVRNet that upsamples the input by  $2\times$ , we randomly crop a patch whose size lies in the range: {128, 144, 160, 176, 192}. For  $4\times$  model, we finetune  $2\times$  model and select random patch size in the range: {64, 72, 80, 88, 96}. Table 3 shows that EVRNet delivers competitive performance as compared to existing methods, but with significantly fewer parameters and MACs. For example, the SSIM score of EVRNet is 0.018 lower than the EDVR, but has  $260\times$  and  $958\times$  fewer parameters and MACs, respectively.

Method	MACs	# Params	PSNR	SSIM
ToFlow [55]	466.83 G	1073.48 K	33.51	0.939
EVRNet (Ours)	10.13 G	78.71 K	32.37	0.921

(a) Vimeo-90K official test set

Method	MACs	# Params	PSNR
V-BM4D <sup>†</sup> [33]	–	–	26.31
DnCNN <sup>†</sup> [59]	128.64 G	588.34 K	26.64
N2V * <sup>†</sup> [25]	140.61 G	27.90 M	25.17
N2N+F2F [58]	–	–	26.56
EVRNet (Ours)	10.13 G	78.71 K	25.79

(b) Vid4 dataset



(c) Qualitative denoising results using EVRNet on Vid4 dataset.

**Table 2: Comparison with state-of-the-art methods on the task of video denoising.** EVRNet is able to denoise videos efficiently. Similar to previous works, we report results in RGB colorspace. Here, <sup>†</sup> represents results are from [58] and \* represents that the number of MACs and parameters are computed for U-Net [40] as N2V is built on top of U-Net. On Vid4 dataset, previous works have not reported SSIM. Therefore, we do not report SSIM on Vid4 dataset.

Method	Up-sampling	MACs	# Params	PSNR	SSIM
ToFlow [55]	$4\times$	466.83 G	1073.48 K	34.83	0.922
DUF [22]	$4\times$	–	–	36.37	0.939
RBPB [11]	$4\times$	29.62 T	12.77 M	37.07	0.944
EDVR [51]	$4\times$	9.96 T	20.10 M	37.61	0.949
EVRNet (Ours)	$4\times$	10.39 G	79.55 K	35.98	0.931
EVRNet (Ours)	$2\times$	10.13 G	78.71 K	37.86	0.965

**Table 3: Comparison with state-of-the-art methods on the task of super-resolution.** EVRNet delivers competitive performance to existing methods, but with significantly fewer multiplication-addition operations (MACs) and network parameters. Similar to previous works, we report results in Y-channel on the official Vimeo-90K test set. See Appendix A.3 for qualitative results.

## 5. Discussion

**Generalization to unseen dataset:** A video transmission system, shown in Figure 1a, compresses the video stream before transmitting to the destination in order to reduce network bandwidth. At the destination, the decoded video stream is of low quality due to compression and transmission noise, and is restored using the video restoration methods. To demonstrate the effectiveness of EVRNet in real-world applications (e.g., real-time video conferencing), we

Seq. Id	# Frames	File Size		RGB		Y-Channel	
		Original	Compressed	PSNR	SSIM	PSNR	SSIM
Seq-1	200	10.7 MB	1.43 MB	37.930	0.966	39.405	0.973
Seq-2	200	35.54 MB	4.60 MB	35.662	0.963	36.730	0.971
Seq-3	200	36.07 MB	4.74 MB	35.880	0.962	36.713	0.967
Seq-4	915	56.66 MB	9.28 MB	38.320	0.976	39.656	0.981
Seq-5	366	11.40 MB	8.05 MB	40.386	0.978	42.536	0.984
Seq-6	821	10.57 MB	7.24 MB	38.775	0.974	40.903	0.979
<b>Avg.</b>				37.826	0.970	39.324	0.976

Table 4: **Quantitative results on unseen videos.** For generating videos with artifacts, videos are first compressed using H264 compression method. A mixed noise (AWGN with  $\sigma^2 = 0.001$  and S&P with  $\rho = 0.1$ ) is then added to synthesize transmission noise. EVRNet is able to remove these artifacts, as is evident in Figure 1b.

Input size	240p		360p		480p	
	240p	480p	360p	720p	480p	960p
iPhone XS	12.7	12.8	7.2	7.8	4.2	4.2
iPhone 11	20.6	20.4	9.2	9.1	5.6	5.7

Table 5: **EVRNet’s speed (in FPS) on edge devices.** Each data point is an average across 100 iterations.

trained “multi-task” EVRNet model that is capable of denoising and deblocking on edge devices (see Figure 1a). To train this model, we used the same training and validation sets as mentioned in Section 4, with an exception to inputs to the model. During training, the input sequences were randomly compressed ( $Q \in [10, 40]$ ). After that, mixed noise ( $\sigma^2 \in [0.001, 0.01]$  and  $\rho \in [0.025, 0.15]$ ) is added to synthesize transmission noise. Each sequence in Vimeo-90K dataset comprises of 8 frames, has a fixed spatial resolution of  $448 \times 256$ , and are compressed frame-by-frame. Therefore, to test the ability of EVRNet in modeling variable-length sequences under both camera and object motion, we evaluated its performance on six high-definition and diverse video sequences that are captured using different mobile devices (see Table 4). For evaluation, we first compressed these videos using H264 encoding and then added a mixed noise (AWGN with  $\sigma^2 = 0.001$  and S&P with  $\rho = 0.1$ ). Quantitative (Table 4) and qualitative (Figure 1b) results shows that EVRNet (1) can model variable-length sequences and (2) generalizes to unseen videos.

**Run-time on edge device:** Typically, video conference applications on edge devices processes 240p and 360p videos at 10-15 frames per second (FPS). To demonstrate the applicability of EVRNet on edge devices, we measured its inference time on two iOS devices: (1) iPhone XS and (2) iPhone 11. Table 5 shows that EVRNet runs in real-time. We would like to highlight that CoreML (Apple’s ML engine) does not support PixelShuffle on the accelerator. To do that operation, we used a solution that uses reshape and transpose operations. These operations are performed on

CU Type	SE Unit	MACs	# Params	RGB		Y-Channel	
				PSNR	SSIM	PSNR	SSIM
Single	✗	9.85 G	68.15 K	31.207	0.868	32.650	0.886
Single	✓	9.85 G	72.95 K	32.006	0.896	33.365	0.914
Multi	✗	10.79 G	73.91 K	29.026	0.875	30.247	0.895
Multi	✓	10.79 G	78.71 K	32.370	0.900	33.679	0.916

(a) Effect of different CU units

Module depth				RGB		Y-Channel		
$N_A$	$N_D$	$N_F$	MACs	# Params	PSNR	SSIM	PSNR	SSIM
1	1	7	11.44 G	78.71 K	31.605	0.887	32.913	0.905
1	7	1	11.44 G	78.71 K	31.753	0.884	32.951	0.901
7	1	1	9.47 G	78.71 K	30.859	0.871	32.139	0.890
2	2	5	11.11 G	78.71 K	32.139	0.901	33.477	0.919
2	5	2	11.11 G	78.71 K	32.057	0.891	33.445	0.908
5	2	2	10.13 G	78.71 K	32.403	0.903	33.884	0.921
3	2	4	10.77 G	78.71 K	31.690	0.890	33.047	0.908
3	4	2	10.77 G	78.71 K	30.785	0.874	32.193	0.896
4	3	2	10.46 G	78.71 K	31.416	0.877	32.690	0.895
3	3	3	10.79 G	78.71 K	32.370	0.900	33.679	0.916

(b) Effect of depth of alignment, differential, and fusion modules

Table 6: **Ablation studies on the task of AWGN denoising** ( $\sigma^2 = 0.001$ ). Overall, EVRNet with multi-scale CUs + SE unit and deeper alignment modules provides the best trade-off between performance and MACs.

iPhone’s CPU (23% CPU occupancy), which resulted in drop in speed. Also, EVRNet is faster on iPhone 11 in comparison to iPhone XS. We believe that accelerator-specific implementations of PixelShuffle along with advancements in hardware technology would further improve the speed of EVRNet on edge devices.

## 6. Ablations

**Effect of different CUs:** Table 6a studies the effect of single- and multi-scale convolutional units (CUs) with and without SE unit on the task of AWGN denoising. Multi-scale CU units with SE improves the performance. We hypothesize that this is because AWGN noise is identically distributed in the frames and kernels at different scales helps learn better representations and remove noisy artifacts (see gray color row in Table 6a).

**Effect of the depth of alignment, differential, and fusion modules:** Table 8 studies EVRNet with different values of  $N_A$ ,  $N_D$ , and  $N_F$ . We are interested in efficient networks for edge devices, therefore, we studied only those combinations that satisfies this criteria:  $N_A + N_D + N_F = 9$ . We found that deeper alignment modules delivers the best trade-off between performance and MACs. Therefore, in our main experiments, we used  $N_A = 5$ ,  $N_D = 2$ , and  $N_F = 2$  (see gray color row in Table 8).

We perform similar studies for deblocking and super-resolution tasks (see Appendix B). We do not observe much gains with different CUs as well as varying the depth of alignment, differential, and fusion modules.



## 7. Conclusion

With virtual presence becoming more and more prominent in present days, it is imperative that video quality is perceptually pleasing which in turn makes the user's experience pleasant. This work introduces EVRNet, a unified network for deblocking, denoising, and super-resolving frames on edge devices. Compared to state-of-the-art video restoration models, EVRNet is more efficient and runs in real-time on edge devices while delivering competitive performance across different tasks. We believe this work will open up new research directions in this area.

## References

- [1] Renzo Andri, Lukas Cavigelli, Davide Rossi, and Luca Benini. Yodann: An architecture for ultralow power binary-weight cnn acceleration. *IEEE Transactions on Computer-Aided Design of Integrated Circuits and Systems*, 2018. 3
- [2] Wenbo Bao, Wei-Sheng Lai, Xiaoyun Zhang, Zhiyong Gao, and Ming-Hsuan Yang. Memc-net: Motion estimation and motion compensation driven neural network for video interpolation and enhancement. *IEEE transactions on pattern analysis and machine intelligence*, 2019. 3
- [3] Jose Caballero, Christian Ledig, Andrew Aitken, Alejandro Acosta, Johannes Totz, Zehan Wang, and Wenzhe Shi. Real-time video super-resolution with spatio-temporal networks and motion compensation. In *Proceedings of the IEEE Conference on Computer Vision and Pattern Recognition*, pages 4778–4787, 2017. 2, 3
- [4] François Chollet. Xception: Deep learning with depthwise separable convolutions. In *Proceedings of the IEEE conference on computer vision and pattern recognition*, pages 1251–1258, 2017. 3
- [5] Guang Deng. A generalized unsharp masking algorithm. *IEEE transactions on Image Processing*, 20(5):1249–1261, 2010. 2, 4
- [6] Chao Dong, Yubin Deng, Chen Change Loy, and Xiaoou Tang. Compression artifacts reduction by a deep convolutional network. In *Proceedings of the IEEE International Conference on Computer Vision*, pages 576–584, 2015. 2, 6
- [7] Chao Dong, Chen Change Loy, Kaiming He, and Xiaoou Tang. Learning a deep convolutional network for image super-resolution. In *European conference on computer vision*, pages 184–199. Springer, 2014. 2
- [8] Alexey Dosovitskiy, Philipp Fischer, Eddy Ilg, Philip Hausser, Caner Hazirbas, Vladimir Golkov, Patrick Van Der Smagt, Daniel Cremers, and Thomas Brox. FlowNet: Learning optical flow with convolutional networks. In *Proceedings of the IEEE international conference on computer vision*, pages 2758–2766, 2015. 3
- [9] Saurabh Gupta, Judy Hoffman, and Jitendra Malik. Cross modal distillation for supervision transfer. In *CVPR*, pages 2827–2836, 2016. 3
- [10] Song Han, Huizi Mao, and William J Dally. Deep compression: Compressing deep neural networks with pruning, trained quantization and huffman coding. In *ICLR*, 2016. 3
- [11] Muhammad Haris, Gregory Shakhnarovich, and Norimichi Ukita. Recurrent back-projection network for video super-resolution. In *Proceedings of the IEEE Conference on Computer Vision and Pattern Recognition*, pages 3897–3906, 2019. 1, 7
- [12] Kaiming He, Xiangyu Zhang, Shaoqing Ren, and Jian Sun. Delving deep into rectifiers: Surpassing human-level performance on imagenet classification. In *Proceedings of the IEEE international conference on computer vision*, pages 1026–1034, 2015. 5
- [13] Kaiming He, Xiangyu Zhang, Shaoqing Ren, and Jian Sun. Deep residual learning for image recognition. In *Proceedings of the IEEE conference on computer vision and pattern recognition*, pages 770–778, 2016. 4
- [14] Yihui He, Ji Lin, Zhijian Liu, Hanrui Wang, Li-Jia Li, and Song Han. Amc: Automl for model compression and acceleration on mobile devices. In *ECCV*, 2018. 3
- [15] Geoffrey Hinton, Oriol Vinyals, and Jeff Dean. Distilling the knowledge in a neural network. In *NIPS Deep Learning and Representation Learning Workshop*, 2015. 3
- [16] Andrew Howard, Mark Sandler, Grace Chu, Liang-Chieh Chen, Bo Chen, Mingxing Tan, Weijun Wang, Yukun Zhu, Ruoming Pang, Vijay Vasudevan, et al. Searching for mobilenetv3. In *Proceedings of the IEEE International Conference on Computer Vision*, pages 1314–1324, 2019. 3, 4
- [17] Andrew G Howard, Menglong Zhu, Bo Chen, Dmitry Kalenichenko, Weijun Wang, Tobias Weyand, Marco Andreetto, and Hartwig Adam. Mobilenets: Efficient convolutional neural networks for mobile vision applications. *arXiv preprint arXiv:1704.04861*, 2017. 3, 4
- [18] Jie Hu, Li Shen, and Gang Sun. Squeeze-and-excitation networks. In *Proceedings of the IEEE conference on computer vision and pattern recognition*, pages 7132–7141, 2018. 4
- [19] Yan Huang, Wei Wang, and Liang Wang. Bidirectional recurrent convolutional networks for multi-frame super-resolution. In *Advances in Neural Information Processing Systems*, pages 235–243, 2015. 2
- [20] Itay Hubara, Matthieu Courbariaux, Daniel Soudry, Ran El-Yaniv, and Yoshua Bengio. Binarized neural networks. In *NIPS*, 2016. 3
- [21] E. Ilg, N. Mayer, T. Saikia, M. Keuper, A. Dosovitskiy, and T. Brox. FlowNet 2.0: Evolution of optical flow estimation with deep networks. In *IEEE Conference on Computer Vision and Pattern Recognition (CVPR)*, Jul 2017. 3
- [22] Younghyun Jo, Seoung Wug Oh, Jaeyeon Kang, and Seon Joo Kim. Deep video super-resolution network using dynamic upsampling filters without explicit motion compensation. In *Proceedings of the IEEE conference on computer vision and pattern recognition*, pages 3224–3232, 2018. 3, 7
- [23] Jiwon Kim, Jung Kwon Lee, and Kyoung Mu Lee. Accurate image super-resolution using very deep convolutional networks. In *Proceedings of the IEEE conference on computer vision and pattern recognition*, pages 1646–1654, 2016. 2
- [24] Diederik P Kingma and Jimmy Ba. Adam: A method for stochastic optimization. *arXiv preprint arXiv:1412.6980*, 2014. 5
- [25] Alexander Krull, Tim-Oliver Buchholz, and Florian Jug. Noise2void-learning denoising from single noisy images. In

- Proceedings of the IEEE Conference on Computer Vision and Pattern Recognition*, pages 2129–2137, 2019. 1, 2, 7
- [26] Christian Ledig, Lucas Theis, Ferenc Huszár, Jose Caballero, Andrew Cunningham, Alejandro Acosta, Andrew Aitken, Alykhan Tejani, Johannes Totz, Zehan Wang, et al. Photo-realistic single image super-resolution using a generative adversarial network. In *Proceedings of the IEEE conference on computer vision and pattern recognition*, pages 4681–4690, 2017. 2
- [27] Chong Li and CJ Richard Shi. Constrained optimization based low-rank approximation of deep neural networks. In *ECCV*, 2018. 3
- [28] Ce Liu and Deqing Sun. A bayesian approach to adaptive video super resolution. In *CVPR 2011*, pages 209–216. IEEE, 2011. 7
- [29] Ding Liu, Zhaowen Wang, Yuchen Fan, Xianming Liu, Zhangyang Wang, Shiyu Chang, and Thomas Huang. Robust video super-resolution with learned temporal dynamics. In *Proceedings of the IEEE International Conference on Computer Vision*, pages 2507–2515, 2017. 2
- [30] Guo Lu, Wanli Ouyang, Dong Xu, Xiaoyun Zhang, Zhiyong Gao, and Ming-Ting Sun. Deep kalman filtering network for video compression artifact reduction. In *Proceedings of the European Conference on Computer Vision (ECCV)*, pages 568–584, 2018. 2, 5, 6
- [31] Bruce D Lucas, Takeo Kanade, et al. An iterative image registration technique with an application to stereo vision. 1981. 2, 3
- [32] Ningning Ma, Xiangyu Zhang, Hai-Tao Zheng, and Jian Sun. Shufflenet v2: Practical guidelines for efficient cnn architecture design. In *Proceedings of the European conference on computer vision (ECCV)*, pages 116–131, 2018. 3
- [33] Matteo Maggioni, Giacomo Boracchi, Alessandro Foi, and Karen Egiazarian. Video denoising, deblocking, and enhancement through separable 4-d nonlocal spatiotemporal transforms. *IEEE Transactions on image processing*, 21(9):3952–3966, 2012. 2, 6, 7
- [34] Sachin Mehta, Mohammad Rastegari, Anat Caspi, Linda Shapiro, and Hannaneh Hajishirzi. Espnet: Efficient spatial pyramid of dilated convolutions for semantic segmentation. In *Proceedings of the european conference on computer vision (ECCV)*, pages 552–568, 2018. 4
- [35] Sachin Mehta, Mohammad Rastegari, Linda Shapiro, and Hannaneh Hajishirzi. Espnetv2: A light-weight, power efficient, and general purpose convolutional neural network. In *Proceedings of the IEEE conference on computer vision and pattern recognition*, pages 9190–9200, 2019. 3, 4
- [36] Pavlo Molchanov, Arun Mallya, Stephen Tyree, Iuri Frosio, and Jan Kautz. Importance estimation for neural network pruning. In *Proceedings of the IEEE Conference on Computer Vision and Pattern Recognition*, pages 11264–11272, 2019. 3
- [37] Andrea Polesel, Giovanni Ramponi, and V John Mathews. Image enhancement via adaptive unsharp masking. *IEEE transactions on image processing*, 9(3):505–510, 2000. 2, 3, 4
- [38] Anurag Ranjan and Michael J Black. Optical flow estimation using a spatial pyramid network. In *Proceedings of the IEEE Conference on Computer Vision and Pattern Recognition*, pages 4161–4170, 2017. 3
- [39] Mohammad Rastegari, Vicente Ordonez, Joseph Redmon, and Ali Farhadi. Xnor-net: Imagenet classification using binary convolutional neural networks. In *ECCV*, 2016. 3
- [40] Olaf Ronneberger, Philipp Fischer, and Thomas Brox. U-net: Convolutional networks for biomedical image segmentation. In *International Conference on Medical image computing and computer-assisted intervention*, pages 234–241. Springer, 2015. 4, 7
- [41] Mehdi SM Sajjadi, Raviteja Vemulapalli, and Matthew Brown. Frame-recurrent video super-resolution. In *Proceedings of the IEEE Conference on Computer Vision and Pattern Recognition*, pages 6626–6634, 2018. 2
- [42] Mark Sandler, Andrew Howard, Menglong Zhu, Andrey Zhmoginov, and Liang-Chieh Chen. Mobilenetv2: Inverted residuals and linear bottlenecks. In *Proceedings of the IEEE conference on computer vision and pattern recognition*, pages 4510–4520, 2018. 3, 4
- [43] Deqing Sun, Xiaodong Yang, Ming-Yu Liu, and Jan Kautz. PWC-Net: CNNs for optical flow using pyramid, warping, and cost volume. In *IEEE Conference on Computer Vision and Pattern Recognition*, 2018. 3
- [44] Christian Szegedy, Sergey Ioffe, Vincent Vanhoucke, and Alex Alemi. Inception-v4, inception-resnet and the impact of residual connections on learning. *arXiv preprint arXiv:1602.07261*, 2016. 4
- [45] Christian Szegedy, Wei Liu, Yangqing Jia, Pierre Sermanet, Scott Reed, Dragomir Anguelov, Dumitru Erhan, Vincent Vanhoucke, and Andrew Rabinovich. Going deeper with convolutions. In *Proceedings of the IEEE conference on computer vision and pattern recognition*, pages 1–9, 2015. 4
- [46] Mingxing Tan, Bo Chen, Ruoming Pang, Vijay Vasudevan, Mark Sandler, Andrew Howard, and Quoc V Le. Mnasnet: Platform-aware neural architecture search for mobile. In *Proceedings of the IEEE Conference on Computer Vision and Pattern Recognition*, pages 2820–2828, 2019. 3
- [47] Mingxing Tan and Quoc V Le. Efficientnet: Rethinking model scaling for convolutional neural networks. *arXiv preprint arXiv:1905.11946*, 2019. 3
- [48] Xin Tao, Hongyun Gao, Renjie Liao, Jue Wang, and Jiaya Jia. Detail-revealing deep video super-resolution. In *Proceedings of the IEEE International Conference on Computer Vision*, pages 4472–4480, 2017. 2
- [49] Yapeng Tian, Yulun Zhang, Yun Fu, and Chenliang Xu. Tdan: Temporally-deformable alignment network for video super-resolution. In *Proceedings of the IEEE/CVF Conference on Computer Vision and Pattern Recognition*, pages 3360–3369, 2020. 3
- [50] Tong Tong, Gen Li, Xiejie Liu, and Qinquan Gao. Image super-resolution using dense skip connections. In *Proceedings of the IEEE International Conference on Computer Vision*, pages 4799–4807, 2017. 2
- [51] Xintao Wang, Kelvin CK Chan, Ke Yu, Chao Dong, and Chen Change Loy. Edvr: Video restoration with enhanced deformable convolutional networks. In *Proceedings of the*

*IEEE Conference on Computer Vision and Pattern Recognition Workshops*, pages 0–0, 2019. 1, 2, 3, 7

- [52] Xintao Wang, Ke Yu, Shixiang Wu, Jinjin Gu, Yihao Liu, Chao Dong, Yu Qiao, and Chen Change Loy. Esrgan: Enhanced super-resolution generative adversarial networks. In *Proceedings of the European Conference on Computer Vision (ECCV)*, pages 0–0, 2018. 2
- [53] Wei Wen, Chunpeng Wu, Yandan Wang, Yiran Chen, and Hai Li. Learning structured sparsity in deep neural networks. In *NIPS*, 2016. 3
- [54] Jiaxiang Wu, Cong Leng, Yuhang Wang, Qinghao Hu, and Jian Cheng. Quantized convolutional neural networks for mobile devices. In *CVPR*, 2016. 3
- [55] Tianfan Xue, Baian Chen, Jiajun Wu, Donglai Wei, and William T Freeman. Video enhancement with task-oriented flow. *International Journal of Computer Vision*, 127(8):1106–1125, 2019. 1, 2, 3, 5, 6, 7
- [56] Junho Yim, Donggyu Joo, Jihoon Bae, and Junmo Kim. A gift from knowledge distillation: Fast optimization, network minimization and transfer learning. In *CVPR*, pages 4133–4141, 2017. 3
- [57] Ruichi Yu, Ang Li, Chun-Fu Chen, Jui-Hsin Lai, Vlad I Morariu, Xintong Han, Mingfei Gao, Ching-Yung Lin, and Larry S Davis. Nisp: Pruning networks using neuron importance score propagation. In *Proceedings of the IEEE Conference on Computer Vision and Pattern Recognition*, pages 9194–9203, 2018. 3
- [58] Songhyun Yu, Bumjun Park, Junwoo Park, and Jechang Jeong. Joint learning of blind video denoising and optical flow estimation. In *Proceedings of the IEEE/CVF Conference on Computer Vision and Pattern Recognition Workshops*, pages 500–501, 2020. 2, 7
- [59] Kai Zhang, Wangmeng Zuo, Yunjin Chen, Deyu Meng, and Lei Zhang. Beyond a gaussian denoiser: Residual learning of deep cnn for image denoising. *IEEE Transactions on Image Processing*, 26(7):3142–3155, 2017. 1, 2, 6, 7
- [60] Barret Zoph and Quoc V Le. Neural architecture search with reinforcement learning. *arXiv preprint arXiv:1611.01578*, 2016. 3

## A. Qualitative results on the Vimeo-90K dataset

### A.1. Deblocking

Figures 7, 8, and 9 demonstrate EVRNet’s ability in deblocking videos at different compression factors in diverse environments ( $Q$ ; lower value of  $Q$  means higher compression). For example, in Figure 7b, EVRNet is able to remove the macro-block artifacts even under high compression ( $Q = 15$ ) around objects (e.g., hand, vegetables, and mixing bowl).

### A.2. Denoising

Figures 10, 11, and 12 demonstrates EVRNet’s ability in denoising different types of noise. For example, in Figure

10c, EVRNet is able to remove the noise and restore videos with high-quality.

### A.3. Video super-resolution ( $4\times$ )

Figure 13 and 14 shows that EVRNet is effective in restoring the details for  $4\times$  video super-resolution. For example, in Figure 14a, EVRNet is able to restore fine details (e.g., hair strands) which are hard to restore with bicubic interpolation.

## B. Ablations

**Effect of different CUs:** Table 7 studies the effect of single- and multi-scale convolutional units (CUs) with and without SE unit. Multi-scale CU units with SE help improve the performance in case of AWGN denoising while no gain was observed in case of deblocking and super-resolution. We hypothesize that this is because compression happens at macro-block level, and both single and multi-scale blocks are able to effectively remove compression artifacts. Unlike macro-block compression, AWGN noise is identically distributed in the frames and kernels at different scales helps learn better representations and remove noisy artifacts (see gray color row in Table 7b).

**Effect of the depth of alignment, differential, and fusion modules:** Table 8 studies EVRNet with different values of  $N_A$ ,  $N_D$ , and  $N_F$ . We are interested in efficient networks for edge devices, therefore, we studied only those combinations that satisfies this criteria:  $N_A + N_D + N_F = 9$ . Similar to the effect of different CUs, we did not observe much gains when varying the depth of alignment, differential, and fusion modules for the task of deblocking and super-resolution. However, for denoising, we found that deeper alignment modules delivers the best trade-off between performance and MACs. Therefore, in our main experiments, we used  $N_A = 5$ ,  $N_D = 2$ , and  $N_F = 2$  (see gray color row in Table 8).



(a) Original



(b) **Left:** Compressed frame ( $Q = 15$ ). **Right:** Deblocked image (RGB PSNR: 31.31 dB)



(c) **Left:** Compressed frame ( $Q = 45$ ). **Right:** Deblocked image (RGB PSNR: 34.79 dB)

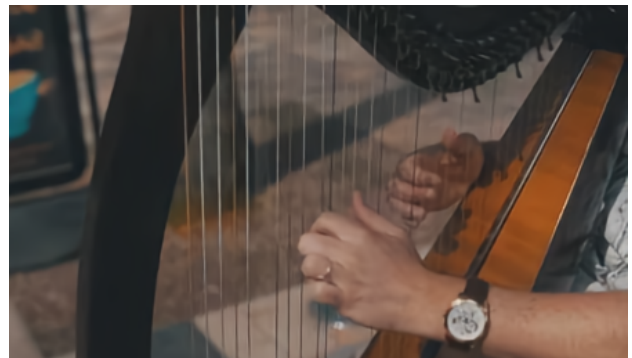
Figure 7: Deblocking example at different values of  $Q$ . Note that lower value of  $Q$  means higher compression.



(a) Original



(b) **Left:** Compressed frame ( $Q = 15$ ). **Right:** Deblocked image (RGB PSNR: 32.11 dB)



(c) **Left:** Compressed frame ( $Q = 45$ ). **Right:** Deblocked image (RGB PSNR: 36.21 dB)

Figure 8: Deblocking example at different values of  $Q$ . Note that lower value of  $Q$  means higher compression.



(a) Original



(b) **Left:** Compressed frame ( $Q = 15$ ). **Right:** Deblocked image (RGB PSNR: 30.23 dB)



(c) **Left:** Compressed frame ( $Q = 45$ ). **Right:** Deblocked image (RGB PSNR: 33.02 dB)

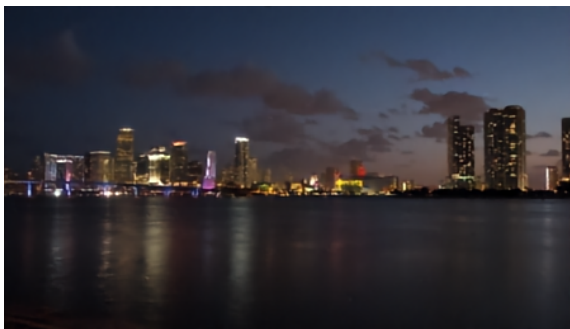
Figure 9: Deblocking example at different values of  $Q$ . Note that lower value of  $Q$  means higher compression.



(a) Original frames



(b) Noised frames with AWGN ( $\sigma^2 = 0.01$ ).



(c) Denoised frames with EVRNet. RGB PSNR of these denoised images is 33.94 dB (**left**) and 37.73 dB (**right**), respectively.

Figure 10: AWGN denoising results on two different sequences.



(a) Original



(b) Noised images with S&P ( $\rho = 0.15$ )



(c) Denoised images with EVRNet. RGB PSNR of denoised images is 37.28 dB and 35.50 dB, respectively.

Figure 11: Salt & Pepper Denoising Example





(a) Original images

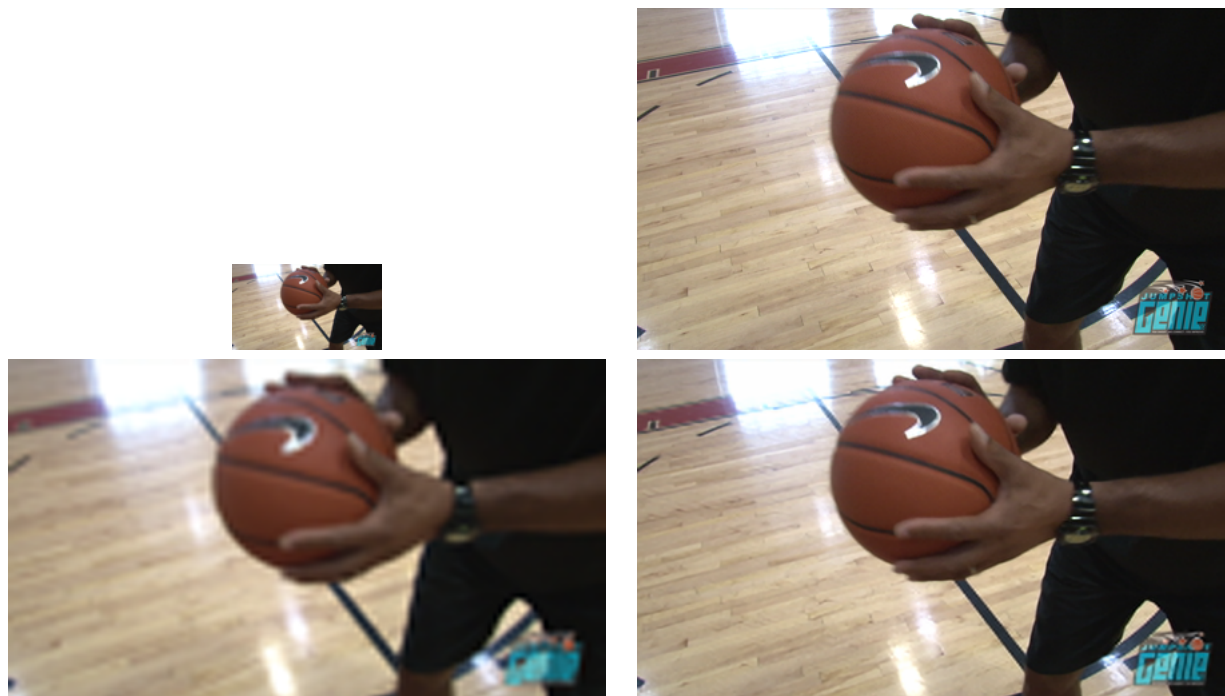


(b) Noised images with AWGN ( $\sigma^2 = 0.001$ ) and S&P ( $\rho = 0.1$ )



(c) Denoised images with EVRNet. RGB PSNR of denoised images is 32.55 dB (left) and 32.09 dB (right), respectively.

Figure 12: Denoising example with mixed noise



(a) **Top left:** Input low-resolution frame. **Top right:** Ground truth. **Bottom left:** Output of bicubic up-sampling (RGB PSNR: 28.59 dB) **Bottom right:** Output of EVRNet (RGB PSNR=34.76 dB).



(b) **Top left:** Input low-resolution frame. **Top right:** Ground truth. **Bottom left:** Output of bicubic up-sampling (RGB PSNR: 27.56 dB) **Bottom right:** Output of EVRNet (RGB PSNR=38.41 dB).

Figure 13: 4× Video super-resolution examples.



(a) **Top left:** Input low-resolution frame. **Top right:** Ground truth. **Bottom left:** Output of bicubic up-sampling (RGB PSNR: 36.84 dB) **Bottom right:** Output of EVRNet (RGB PSNR=42.84 dB).



(b) **Top left:** Input low-resolution frame. **Top right:** Ground truth. **Bottom left:** Output of bicubic up-sampling (RGB PSNR: 36.21 dB) **Bottom right:** Output of EVRNet (RGB PSNR=43.97 dB).

Figure 14: 4× Video super-resolution examples.

CU Type	SE Unit	MACs	# Params	RGB		Y-Channel	
				PSNR	SSIM	PSNR	SSIM
Single	✗	9.85 G	68.15 K	36.358	0.948	38.477	0.961
Single	✓	9.85 G	72.95 K	36.323	0.948	38.403	0.961
Multi	✗	10.79 G	73.91 K	36.297	0.947	38.363	0.961
Multi	✓	10.79 G	78.71 K	36.334	0.948	38.478	0.962

(a) Deblocking ( $Q = 40$ )

CU Type	SE Unit	MACs	# Params	RGB		Y-Channel	
				PSNR	SSIM	PSNR	SSIM
Single	✗	9.85 G	68.15 K	31.207	0.868	32.650	0.886
Single	✓	9.85 G	72.95 K	32.006	0.896	33.365	0.914
Multi	✗	10.79 G	73.91 K	29.026	0.875	30.247	0.895
Multi	✓	10.79 G	78.71 K	32.370	0.900	33.679	0.916

(b) AWGN Denoising ( $\sigma^2 = 0.001$ )

CU Type	SE Unit	MACs	# Params	RGB		Y-Channel	
				PSNR	SSIM	PSNR	SSIM
Single	✗	9.90 G	68.33 K	37.406	0.962	38.042	0.966
Single	✓	9.90 G	73.14 K	37.318	0.962	37.955	0.965
Multi	✗	10.84 G	74.10 K	37.181	0.962	37.868	0.966
Multi	✓	10.84 G	78.91 K	37.378	0.962	38.002	0.966

(c) Super-resolution ( $2\times$ )

Table 7: **Effect of different CU units.** Multi-scale blocks are effective in restoring fine-grained details (e.g., noise) while both single- and multi-scale blocks are effective in restoring block-level artifacts (e.g., compression). Here, we used  $N_A = N_D = N_F = 3$ .

Module depth			MACs	# Params	RGB		Y-Channel	
$N_A$	$N_D$	$N_F$			PSNR	SSIM	PSNR	SSIM
1	1	7	11.44 G	78.71 K	36.320	0.948	38.411	0.961
1	7	1	11.44 G	78.71 K	36.356	0.948	38.450	0.962
7	1	1	9.47 G	78.71 K	36.334	0.948	38.472	0.961
2	2	5	11.11 G	78.71 K	36.200	0.946	38.297	0.960
2	5	2	11.11 G	78.71 K	36.327	0.948	38.412	0.962
5	2	2	10.13 G	78.71 K	36.307	0.947	38.403	0.961
3	2	4	10.77 G	78.71 K	36.359	0.948	38.451	0.962
3	4	2	10.77 G	78.71 K	36.307	0.947	38.390	0.961
4	3	2	10.46 G	78.71 K	36.287	0.948	38.405	0.961
3	3	3	10.79 G	78.71 K	36.334	0.948	38.478	0.962

(a) Deblocking ( $Q = 40$ )

Module depth			MACs	# Params	RGB		Y-Channel	
$N_A$	$N_D$	$N_F$			PSNR	SSIM	PSNR	SSIM
1	1	7	11.44 G	78.71 K	31.605	0.887	32.913	0.905
1	7	1	11.44 G	78.71 K	31.753	0.884	32.951	0.901
7	1	1	9.47 G	78.71 K	30.859	0.871	32.139	0.890
2	2	5	11.11 G	78.71 K	32.139	0.901	33.477	0.919
2	5	2	11.11 G	78.71 K	32.057	0.891	33.445	0.908
5	2	2	10.13 G	78.71 K	32.403	0.903	33.884	0.921
3	2	4	10.77 G	78.71 K	31.690	0.890	33.047	0.908
3	4	2	10.77 G	78.71 K	30.785	0.874	32.193	0.896
4	3	2	10.46 G	78.71 K	31.416	0.877	32.690	0.895
3	3	3	10.79 G	78.71 K	32.370	0.900	33.679	0.916

(b) AWGN Denoising ( $\sigma^2 = 0.001$ )

Module depth			MACs	# Params	RGB		Y-Channel	
$N_A$	$N_D$	$N_F$			PSNR	SSIM	PSNR	SSIM
1	1	7	11.50 G	78.91 K	37.071	0.961	37.742	0.965
1	7	1	11.50 G	78.91 K	37.136	0.961	37.774	0.965
7	1	1	9.52 G	78.91 K	37.176	0.961	37.868	0.965
2	2	5	11.17 G	78.91 K	37.072	0.961	37.740	0.965
2	5	2	11.17 G	78.91 K	37.102	0.961	37.776	0.965
5	2	2	10.18 G	78.91 K	37.196	0.961	37.855	0.965
3	2	4	10.84 G	78.91 K	37.227	0.962	37.902	0.965
3	4	2	10.84 G	78.91 K	37.071	0.961	37.740	0.965
4	3	2	10.51 G	78.91 K	37.173	0.961	37.877	0.965
3	3	3	10.84 G	78.91 K	37.378	0.962	38.002	0.966

(c) Super-resolution ( $2\times$ )

Table 8: **Effect of the depth of alignment, differential, and fusion modules in the EVRNet.** Overall, EVRNet with deeper alignment modules provides the best trade-off between performance and number of multiplication-addition operations (MACs). In all these models, the depth of the network is fixed, i.e.,  $N_A + N_D + N_F = 9$ .